# CHAPTER 4

# DESIGN, ANALYSIS AND PERFORMANCE STUDY OF A FOUR-CAVITY 35 GHz GYROKLYSTRON AMPLIFIER

## 4.1 Introduction

Gyroklystron is a stable millimeter-wave amplifier used for a variety of applications, including particle acceleration, plasma heating, high resolution and long range radars. The frequency of operation of gyroklystrons ranges from millimeter wave to the terahertz wave range. Though it is inherently a narrow-band device, it has the advantage of giving a high gain. The interaction structure of the gyroklystron consists of a series of uncoupled cavities that provide the necessary RF field for interaction with the electron beam passing azimuthally through the structure. The RF signal to be amplified is fed into the first cavity, called buncher cavity, using some suitable coupling mechanism. The amplitude of the signal increases as it is induced in successive cavities due to the relativistic mechanism known as CRM instability, which cause phase modulation of accelerated electrons followed by their density modulation in the drift tubes. The amplified signal is coupled out to load from the last cavity, also called the catcher cavity. The gain of the signal depends upon the number of cavities used with approximately a gain of 10 dB per cavity. The purpose of the present chapter is to identify important design parameters for the design of gyroklystron amplifier and to develop a suitable approach for its design. As, in most of the reported work, detailed description of device design methodology and beam-wave interaction mechanism at the different locations within the device of a gyroklystron amplifier are not available. Therefore, in the present work, a comprehensive device design methodology is given, and a systematic design of a typical 35 GHz four-cavity gyroklystron amplifier operating at the fundamental mode is explained. Further, this device design is validated through the PIC simulation and nonlinear analysis. In addition, a practical problem of misalignment of the RF cavities with drift tubes within the tube is also investigated and its effect on device performance is also studied.

## 4.2 Design Methodology

The process of designing a gyroklystron includes the choice of the desired RF operating mode correspondingly the RF interaction structure, electron beam

parameter, and magnetic field selections. The finalization of the RF interaction structure consists of several steps. First, the resonance frequency and quality factor with a desired field profile of each cavity are chosen. Based on this information, cavities shapes, sizes and connecting drift tube radii are chosen. After this the various device input parameters, such as beam voltage, beam current, transverse to axial beam velocity ratio (pitch factor), guiding center, radius and magnetic field values are judiciously chosen with the help of its parametric analysis to achieve the goal efficiency and power. The beam current and the magnetic field are mainly decided by the start oscillation current criteria study necessary for the stable operation of the device. Since gyroklystron is an amplifier, therefore, its operating current value is chosen such that it should be always less than the start oscillation current. The coupling coefficient curves help us to decide the optimum beam radius for maximum beam to mode coupling.

### 4.2.1 Mode selection

For the device operation at the specific frequency, it is necessary that the device should work in that particular mode. The device operation in the parasitic modes results in a shift in its operating frequency and also a decrease in the efficiency. In order to ensure to the design mode excitation, various factors have to be considered in a gyroklystron amplifier. The choice of operating mode depends on the ohmic wall losses, mode competition, feasibility of the electron gun cathode design and coupling coefficient. To accommodate the large peak power, all the cavities of gyroklystron should be designed for stable operation in the desired mode.

For the operation in $TE_{mn}$ mode, the cavity wall radius ($r_w$) is related to $\lambda$ by

$$r_w = \left(v_{mn}\,\lambda/2\pi\right) \quad , \tag{4.1}$$

where, $v_{mn}$ is the $n^{\text{th}}$ root of the first derivative of Bessel function $\left(J'_m(x)\right)=0$. The optimum electron beam radius is given by:

$$r_b = \left(v_{m\pm s,i}\,r_w/v_{mn}\right) = \left(v_{m\pm s,i}\lambda/2\pi\right) \qquad (i = 1\text{or } 2)\,, \tag{4.2}$$

where, $s$ is the harmonic number. In general, the co-rotating mode (with the lower sign) is chosen since this provides better coupling of the electron beam to the RF field [Kartikeyan *et al*. (2004)].

The drift tubes are also designed for the stable operation of the device by making them cutoff to the operating mode. The drift radius ($r_d$) should be small enough that all modes are cutoff. On the other hand, drift radius should be adequately large that the electron beam passes through it without any interception. However, both the conditions cannot be fully satisfied simultaneously. Therefore, a trade-off is required between realistic estimates and design goal to fix the drift tube radius. Thus, the drift tube radius must be small enough so that the operating mode is cutoff to the chosen radius. These requirements set the condition for choosing the drift radius as $r_b<r_d<r_w$ for an operating mode.

The length of the drift tube is decided by keeping the fact that at least 40 dB isolation is required between the two gyroklystron cavities to avoid any crosstalk between them. The approximate expression for the drift tube length ($L_d$) can be obtained by using the cold-cavity dispersion relation [Chu *et al*. (1985)]:

$$k_{\|}^2 = \left(\frac{v_{mn}}{r_d}\right)^2 - \left(\frac{\omega}{c}\right)^2 \quad . \tag{4.3}$$

An isolation of 40 dB requires that $e^{-2k_{\|}L_d} < 10^{-4}$, where $L_d$ is the drift tube length. In the simplest form this inequality can be rewritten as:

$$L_d > \frac{4.6}{\left(\frac{v_{mn}}{r_d}\right)^2 - \left(\frac{\omega}{c}\right)^2} \quad . \tag{4.4}$$

### 4.2.2 Coupling coefficient

The coupling coefficient determines the strength of the electron beam coupling to the RF mode and depends on the electron beam guiding center radius and the electric field distribution for a particular mode. The coupling coefficient should be maximum for the selected mode, so that the desired mode can be excited during the device operation. Once the desired mode is excited properly by the helical moving electron beam, the other competing modes are suppressed, and

power growth mechanism gets single mode stability. The coupling coefficient between the electron beam and RF fields in the cylindrical cavities is defined as:

$$C_{mn} = \frac{J_{m\pm s}^2(k_\perp r_b)}{(v_{mn}^2 - m^2)J_m^2(v_{mn})} \quad , \tag{4.5}$$

where, $k_\perp = 2\pi/\lambda$, $r_b$ is the beam radius, $v_{mn}$ is the eigenvalue of the *mn* mode.

Using the above expression, we can find the optimum electron beam launching position to have maximum coupling for the chosen mode. The normalized coupling coefficient ($C_{mn}$) with respect to the normalized beam radius for the different number of modes is shown in Fig. 4.1. It can be seen from the Fig. 4.1, that the coupling coefficient $C_{mn}$ between the electron beam and RF field in the cavities in case of $TE_{01}$ mode is much larger than that of all other modes. So, in order to have the maximum interaction between the electron beam and the electromagnetic field, the $TE_{01}$ mode is chosen as the operating mode in each cavity. The first radial maximum of $TE_{01}$ mode, which is equal to normalized beam radius and found as 0.5, is the normalized beam position for maximum coupling.

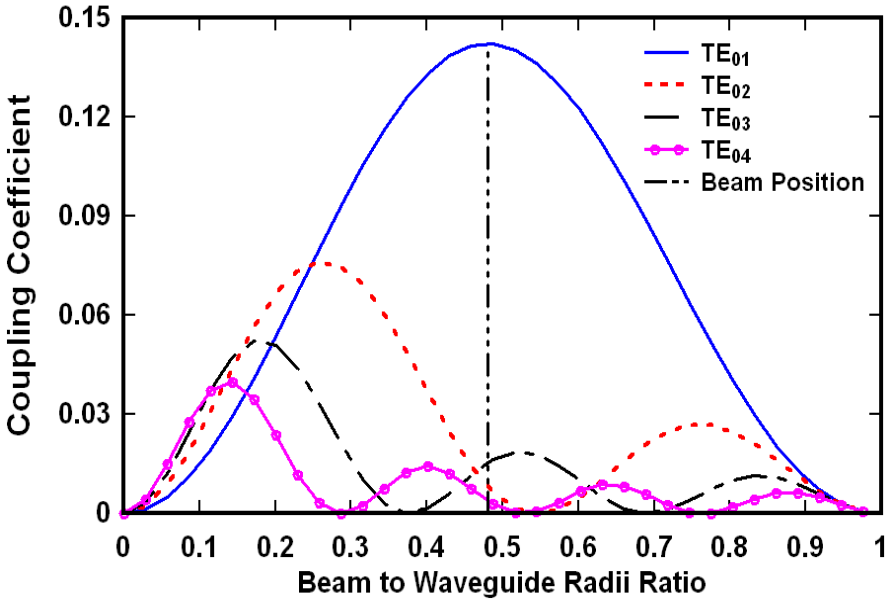


**Fig. 4.1** Coupling coefficient $C_{mn}$ as a function of ratio of beam to waveguide radii ($r_b/r_w$) for the different modes.

### 4.2.3 Wall loading

Ohmic loss is one of the major constraints in the operation of high power gyroklystrons. This electromagnetic power loss occurs in the cavities as the ohmic heating due to the finite conductivity of the cavity material. In a multicavity gyroklystron, wall losses are more significant in the output cavity as maximum RF power is generated in the output cavity due to the strong beam-wave interaction by which electron loses its energy to RF in the output cavity. For calculating the wall losses one must have an idea about the RF output power and the quality factor ($Q$) of the cavity. These two quantities have to be fixed before calculating the ohmic losses in the cavity. The ohmic loss density on the cavity wall can be calculated as [Kreischer *et al*. (1985)]:

$$\rho_{ohm} = \frac{1}{2\sigma\delta}\left|\hat{n}\times H\right|^2_{r=r_b} = \frac{1}{2\sigma\delta_d\mu_0^2}\left(1+\frac{m^2k_z^2}{k_{mn}^4 r_b^2}\right)\frac{k_{mn}^2}{\omega^2}E_0^2 J_m^2(k_{mn}r_b)\left|f(z)\right|^2 \tag{4.6}$$

where $\delta_d$ is the skin depth, $\sigma$ is the electrical conductivity of the cavity wall. The second term in the bracket is negligible in the cutoff limit $k_{\|} \ll k_{\perp}$. This expression of ohmic loss density can be expressed in terms of the normalized field amplitude parameter $F$, and detuning parameter $\Delta$ as [Kreischer *et al*. (1985)]

$$\rho_{ohm}(W/m^2) = 5.1\times10^{-15}\sigma^{-0.5}\omega^{2.5}F^2\beta_{\perp}^6 C_t^2\gamma^2(1-0.5\beta_{\perp}^2\Delta)^2 \tag{4.7}$$

where, $C_t = \dfrac{J_m(v_{mn})}{J_{m\pm s}(k_{\perp}r_b)}$. This will provide the choice of the cathode voltage and field amplitude for a tolerable wall loss. For a Gaussian axial profile function, $f(z) = \exp(-4z^2/L^2)$ the stored energy in the cavity is:

$$U_w = \varepsilon_0 E_0^2\left(\frac{\pi}{2}\right)^{3/2}\frac{L}{2k_{mn}^2}\left(v_{mn}^2 - m^2\right)J_m^2(v_{mn}) \tag{4.8}$$

On combining the above two equations, the equation relating the cavity mode indices to the ohmic loss density for a given power ($P$) can be expressed as:

$$\begin{aligned}\left(v_{mn}^2 - m^2\right) &= \frac{16\pi}{c^3}\sqrt{\frac{2}{\sigma\mu_0}}\left(\frac{L}{\lambda}\right)\frac{Pf^{5/2}}{(1-R_2)\rho_{ohm}} \\ &= 1.05\times10^{-3}\left(\frac{L}{\lambda}\right)\frac{P(MW)f^{5/2}(GHz)}{(1-R_2)\rho_{ohm}(kW/cm^2)}\end{aligned} \tag{4.9}$$

The maximum wall losses defined in terms of (heat dissipated per unit area) *dP/ dA* can be estimated as

$$\left(\frac{dP}{dA}\right)_{\max} \approx \sqrt{\frac{8}{\pi}}\sqrt{\frac{1}{\pi Z_0 \sigma}}\frac{PQ}{L\lambda^{1.5}}\frac{1}{x_{mn}^2 - m^2} \quad , \tag{4.10}$$

where $L$ is the length parameter of the individual cavity, $P$ is the power in the cavity, $Q$ is the total quality factor of the cavity, and $Z_0 = 377\ \Omega$ is the impedance of the free space.

**Table 4.1** Wall loading for different modes.

| $m$ | $n$ | $\nu_{mn}$ | $dP/dA$ $(kW/cm^2)$ |
|---|---|---|---|
| **0** | **1** | **3.831** | **0.1885** |
| **0** | **2** | **7.015** | **0.0562** |
| **1** | **1** | **1.841** | **0.8163** |
| **1** | **2** | **5.331** | **0.0974** |
| **2** | **1** | **3.054** | **0.2966** |
| **2** | **2** | **6.706** | **0.0615** |
| **0** | **3** | **10.173** | **0.0267** |
| **0** | **4** | **13.323** | **0.0156** |

Table 4.1 shows the wall losses calculated for the different number of modes. From the Table 4.1, clearly the wall loading for the selected $TE_{01}$ mode is well below the limitation (i.e. <2 kW/cm$^{2)}$. Figure 4.2 shows the trade-off between mode eigenvalue and the wall loss with the maximum output power as a parameter for input cavity, second cavity, penultimate cavity and output cavity. For the $TE_{01}$ mode of operation and 200 kW of output power, wall losses of all the four cavities of the present gyroklystron amplifier are less than the specified limit 2 kW/cm$^2$, which confirms the selection of $TE_{01}$ mode as an operating mode, an appropriate choice for the gyroklystron amplifier under consideration.

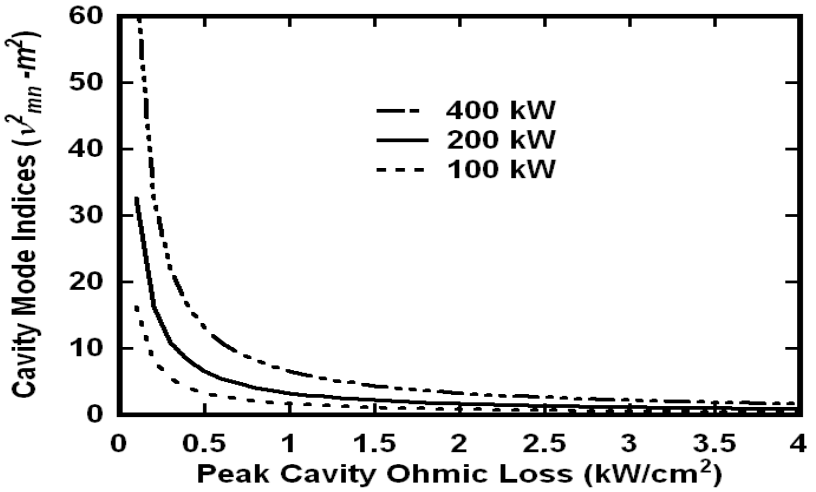


(a)

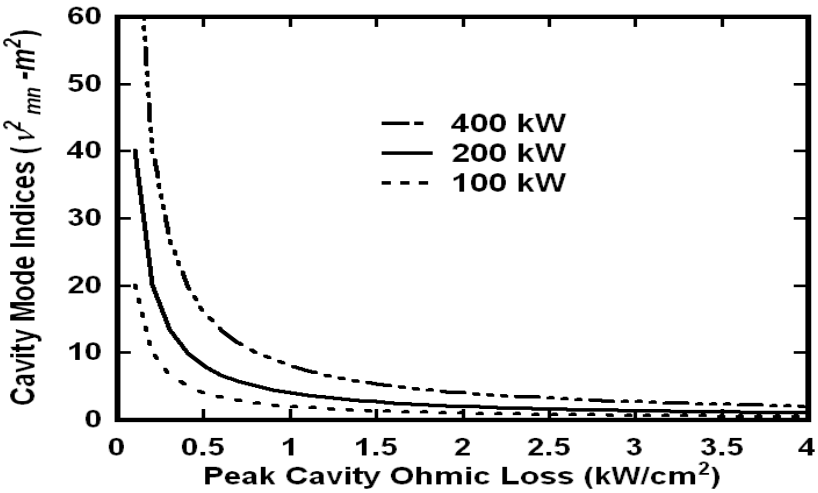


(b)

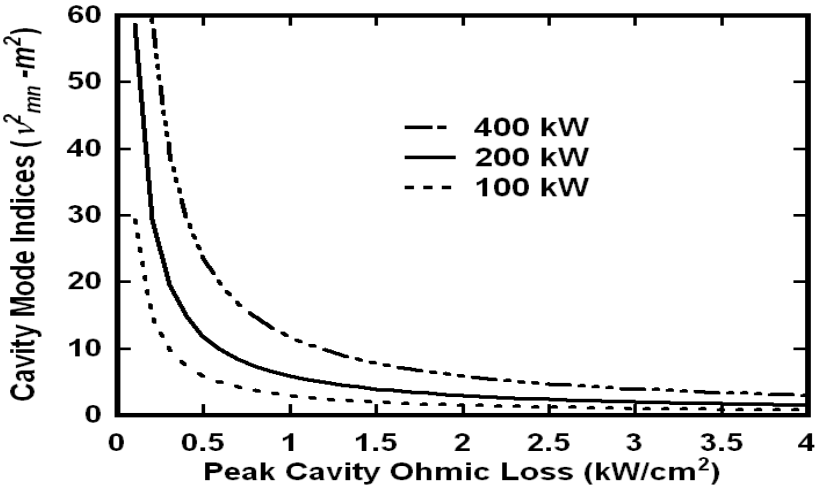


(c)

**Fig. 4.2** Cavity mode indices versus ohmic power loss density with output power as a parameter for (a) input cavity, (b) second and third cavities, and (c) output cavity.

### 4.2.4 Start oscillation current

The start oscillation current is the current at which the cavity starts oscillating even in the absence of any driver signal. For efficient operation of gyroklystron amplifier, it is necessary that the operating current should be less than the start oscillation current which depends on the beam properties, cavity dimensions, cavity $Q$'s and the magnetic field. It is also important to estimate the start oscillation current of various possible competing modes. By calculating and comparing the start oscillation current of desired and competing modes, it is ensured that the required mode is excited with maximum efficiency at the desired power level, thus suppressing the unwanted modes. Considering the Gaussian profile, the normalized start oscillation current in terms of $\mu$ and $\Delta$ is given by [Fliflet *et al.* (1982), Gold *et al.* (1990)]:

$$\hat{I}_{st}(\mu,\Delta) = (4/\pi\mu^2)[e^{2x^2}/(\mu x - s)] \quad , \tag{4.11}$$

where, $x = \mu\Delta/4$, $\mu$ is the normalized interaction length of the cavity, $\Delta$ is the detuning parameter and $s$ is the harmonic number. The actual start oscillation current is calculated by putting the normalized beam current equal to the normalized start oscillation current and is thus given by:

$$I_{st} = \left(\frac{\pi^{5/2}}{\sqrt{2}}\right)\frac{c^3 m_e \varepsilon_0}{e}\frac{\beta_{\perp 0}^4 \gamma_0}{Q}\frac{L}{\lambda}\frac{\hat{I}_{st}}{C_{mn}} \quad , \tag{4.12}$$

where $C_{mn}$ is the coupling coefficient defined by equation (4.5), and $Q$ is the loaded quality factor.

The start oscillation current shown in Fig. 4.3 is calculated for $TE_{01}$ and the nearby competing modes typically for a 35 GHz gyroklystron amplifier with respect to magnetic field $B_0$ to investigate the stability condition of the designed gyroklystron amplifier. It can be observed from Fig. 4.3 that the start oscillation current ($I_{st}$) for input cavity is around 12 A. Hence, the cavity is stable for any operating current values chosen below the start oscillation current at the operating magnetic field. Figure 4.4 shows the effect of electron beam pitch factor (α) on the stability of the operating $TE_{01}$ mode in the input cavity. With increase in α,

the stability of the RF cavity decreases due to the decrease in the start oscillation current values.

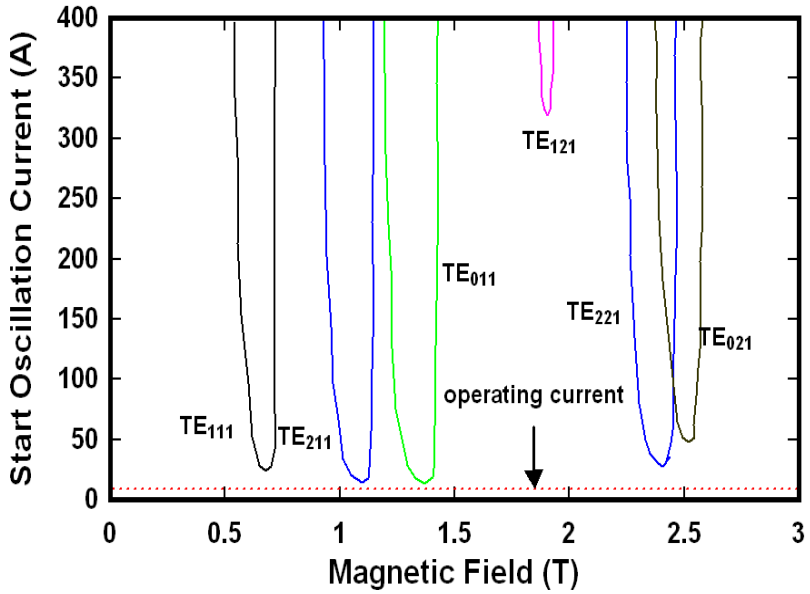


**Fig. 4.3** Start oscillation current versus operating DC magnetic field for the different nearby competiting modes.

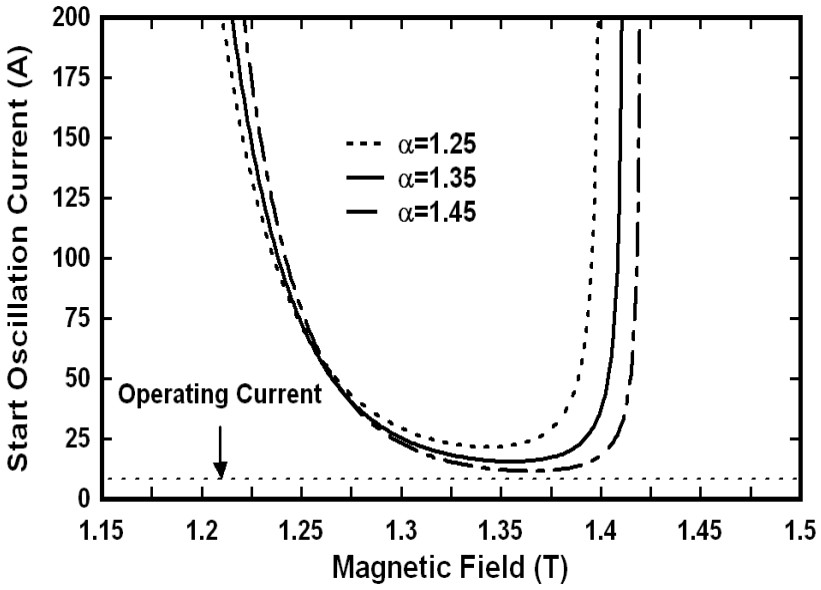


**Fig. 4.4** Start oscillation current versus operating DC magnetic field for $TE_{01}$ mode for different values of beam pitch factor (α).

### 4.2.5 Space charge effects

The space charge effect is a common phenomenon which occurs during the electron beam transportation. This effect is created due to the potential of the transported charge beam. The space charge effect mainly depends on the electron beam geometry and the structure geometry through which the electron beam is moving. The space charge effect can be defined in terms of the voltage depression ($V_d$) and the limiting current ($I_L$). In case of a gyroklystron amplifier, the helical electron beam drifts through a series of cylindrical RF interaction cavities separated by drift tubes and hence, space charge effects are produced during the electron beam transportation from the input cavity to the output cavity. For the effective operation of a gyroklystron amplifier, the voltage depression likely to be small and the limiting current should be high as much possible. The limiting current is defined as the current which can be easily transported through the interaction structure. If the current beyond the limiting current value is allowed to pass through the interaction structure, the voltage depression becomes so high that the mirroring of the electron beam occurs, whereas the normalized axial velocity component of the electron beam becomes zero ($\beta_{\|} \to 0$). As a consequence of which, the electron beam will be no longer propagates in axial direction and is reflected back. However, in the case of a gyroklystron amplifier, the operating current is well below the limiting current. As, for the stable operation of a gyroklystron as an amplifier, the necessary condition for beam current is $I_b<I_{st}<I_L$, but the space charge effects due to voltage depression may still be significant. A reduction in efficiency of the device results because the voltage depression reduces the energy available for conversion to RF waves. Further, additional loss in efficiency will be caused by the spread in beam energy produced by the potential drop across the beam. The upper limit for the voltage depression is roughly estimated to be around 10% of the applied beam voltage, and the cutoff point of the limiting current is around twice the operating beam current. The effect of voltage depression can be reduced to an extent by increasing the beam voltage, and by making use of depressed collector [Chu *et al.* (1985), Ganguly *et al.* (1984), Kartikeyan *et al.* (2004)]. The voltage depression

($V_d$) and the limiting current ($I_L$) can be mathematically expressed as follows [Ganguly *et al*. (1984), Kartikeyan *et al*. (2004)]

$$V_d \approx 60 \frac{I_b}{\beta_{\|}} \ln\left(\frac{r_w}{r_b}\right) \quad , \tag{4.13}$$

$$I_L \approx 8500 A \left[\gamma^* / \ln\left(\frac{r_w}{r_b}\right)\right] \quad , \tag{4.14}$$

where, $\gamma^* = \gamma_0 \left[1-\left(1-\beta_{\|0}^2\right)^{1/3}\right]^{3/2}$, $I_b$ is the beam current, $\beta_{\|0}$ is the value of $\beta_{\|}$ and $\gamma_0$ is the relativistic factor at the inlet of the input cavity respectively. From equations, (4.13) and (4.14) it is clear that the voltage depression and the limiting current depends mainly on the beam radius and the cavity wall radius. Moreover, from equations (4.1) and (4.2), it is evident that the beam radius and the cavity wall radius are selected on the basis of operating mode and thus, the space charge effect in the gyroklystron interaction cavities can be easily controlled by making a proper choice of operating mode.

Figure 4.5 shows the dependence of voltage depression on beam voltage for different values of beam current. It is quite evident from Fig. 4.5 that at the high beam current operation, voltage depression increases, which result in reduction of device efficiency due to the potential drop and beam energy spread effects caused by the voltage depression.

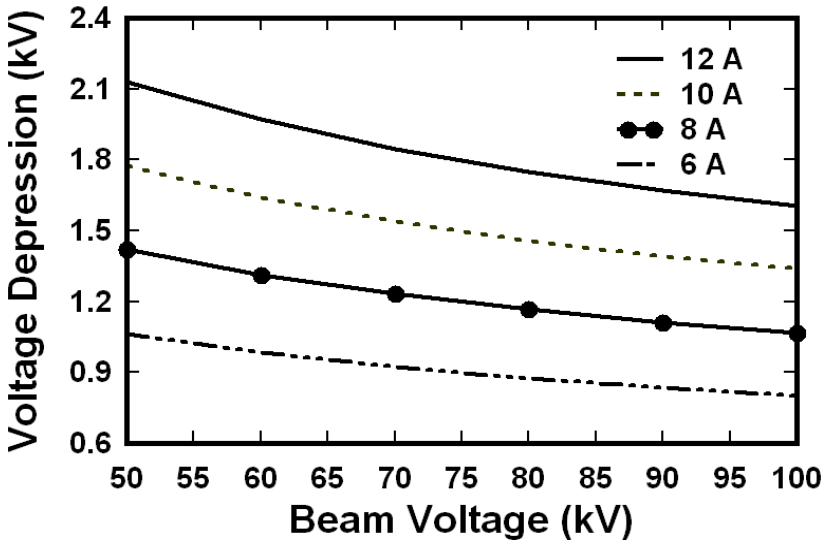


**Fig. 4.5** Voltage depression versus beam voltage for different values of beam current.

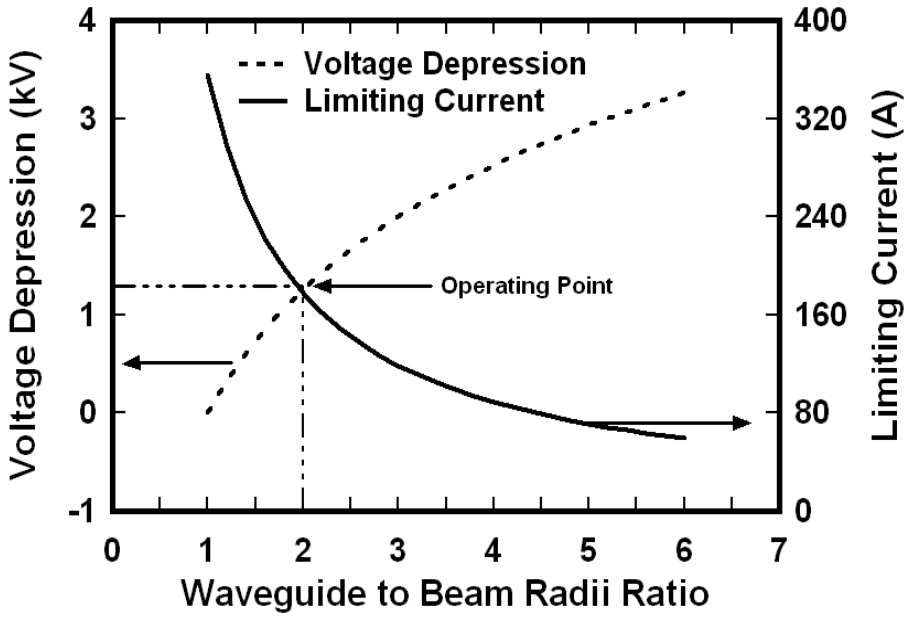


**Fig. 4.6** Voltage depression and limiting current versus the ratio of waveguide to beam radii ($r_w/r_b$).

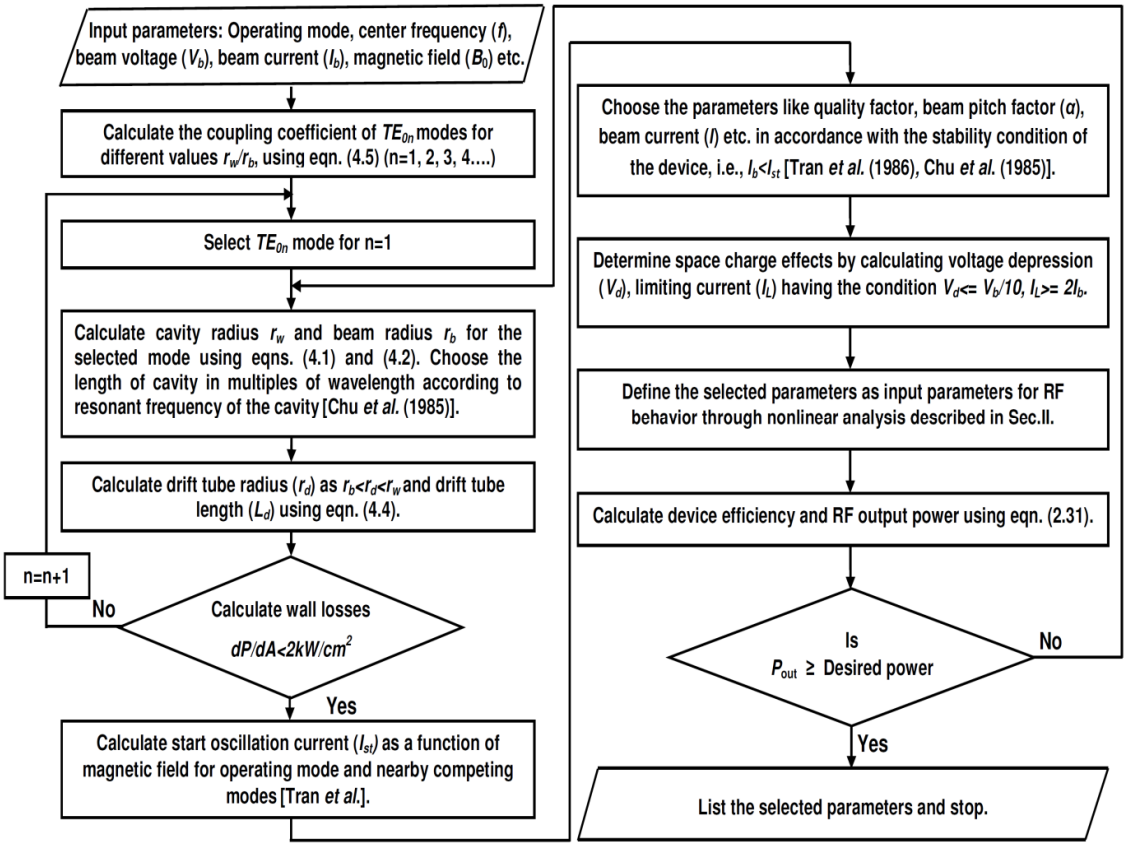


**Fig. 4.7** Flow chart describing the gyroklystron design procedure.

Figure 4.6 shows, the voltage depression and the limiting current variations respectively as a function of the cavity wall to the electron beam radii ratio ($r_w/r_b$). The voltage depression increases with the ratio of cavity to electron beam radii ($r_w/r_b$), while the limiting current decreases. For, the chosen operating point the ratio of cavity to electron beam radii ($r_w/r_b$=2), voltage depression is around 1.2 kV whereas the value of limiting current is around 200 A. It means for the selected $TE_{01}$ mode, the space charge effects are within the limits for chosen beam voltage 70 kV and beam current 8 A. Subsequently, the parameters selected above are used as input parameters for the beam-wave interaction behavior study through nonlinear analysis described in Chapter 2. The efficiency and RF output power of the device is estimated using equation (2.31) and parameters are optimized for the optimum performance in terms of efficiency and RF output power. The flow chart for the design methodology of gyroklystron amplifier used in the present chapter is shown in Fig. 4.7.

**Table 4.2** Design specifications for 35 GHz, 200 kW four-cavity gyroklystron amplifier

| Particulars | Specifications |
|---|---|
| **Mode** | **$TE_{01}$** |
| **Beam Voltage ($V_b$)** | **70 kV** |
| **Beam Current ($I_b$)** | **8.2 A** |
| **DC Magnetic field ($B_0$)** | **1.34 T** |
| **Velocity ratio** | **1.45** |
| **Input Cavity Length** | **12.85 mm** |
| **Second Cavity Length** | **15.86 mm** |
| **Third Cavity Length** | **15.86 mm** |
| **Output Cavity Length** | **23.14 mm** |
| **Drift Tube Length** | **14.57 mm** |
| **Drift Tube Radius** | **4.1 mm** |
| **Wall Loading** | **<2.0 kW/cm$^2$** |
| **Quality Factor** | **192** |

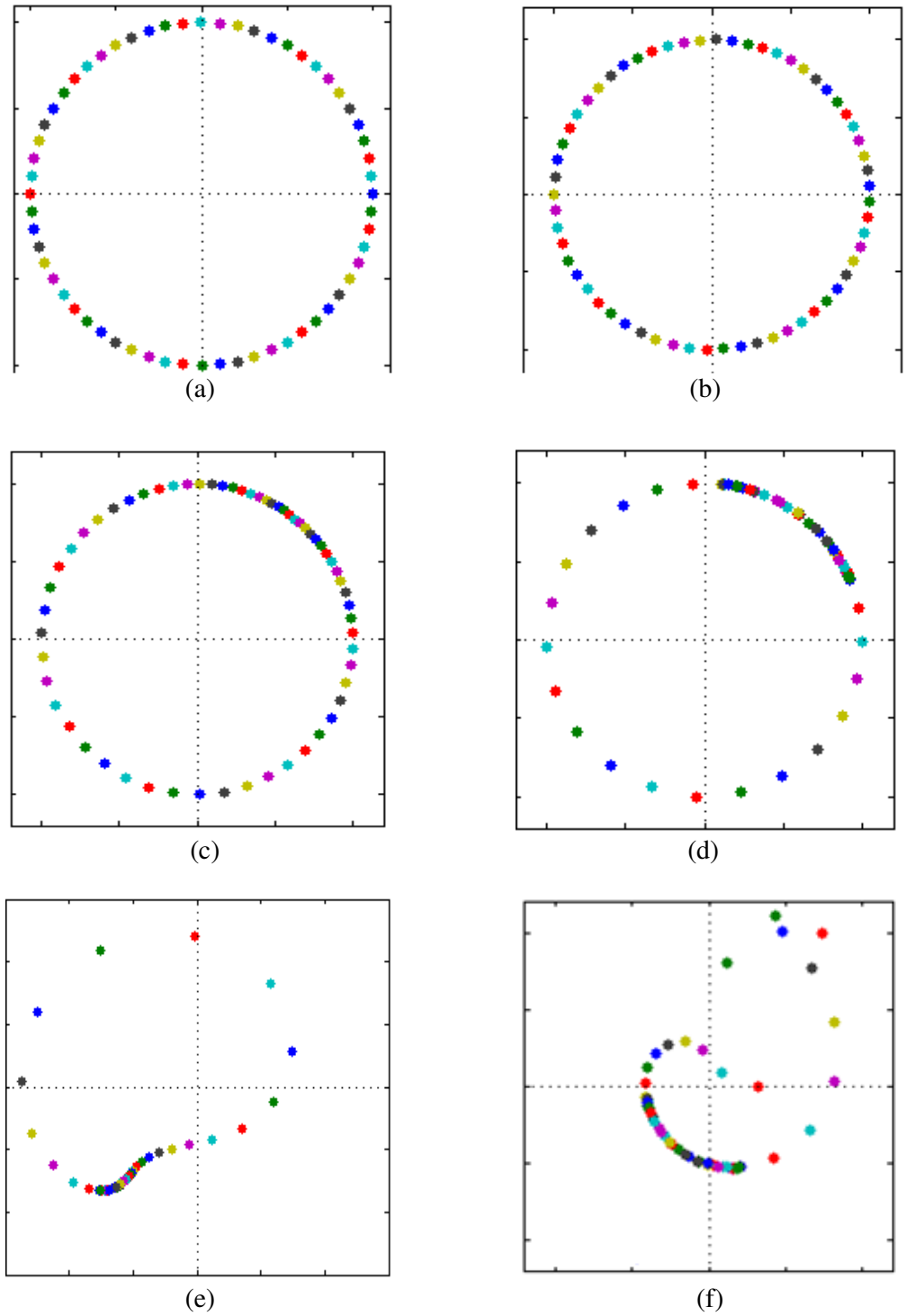


**Fig. 4.8** Electrons phase distribution at different positions in phase space (a) inlet of the input cavity (b) inlet of the second cavity (c) inlet of the penultimate cavity (d) inlet of the output cavity (e) middle of the output cavity, and (f) outlet of the output cavity.

## 4.3 Nonlinear Analysis

Based on the design methodology discussed above, the design parameters of a typical selected 35 GHz gyroklystron amplifier have been finalized. In comparison to the four-cavity gyroklystron amplifier reported by Garven *et al.,* the present gyroklystron amplifier is designed to be operated at high efficiency by selecting the device operation at higher electron transverse to axial velocity ratio ($\alpha$). The stability of the device decreases due to its operation at higher values of electron transverse to axial velocity ratio because of decrease in start oscillation current. Therefore, lower value of operating beam current has been selected compared to the device reported by Garven *et al*. For the design of a 35 GHz four-cavity gyroklystron amplifier having 200 kW RF power output with 45 dB gain, the initial estimation of the beam current ($I_b$) and beam voltage ($V_b$) is done on the basis of the required output power (200 kW) and keeping efficiency of the device ~ 35%. The initial beam current ($I_b$) and the beam voltage ($V_b$) for the present gyroklystron were taken as 8.5 A and 67 kV respectively. These initial values of the beam current and beam voltage were further optimized using the nonlinear analysis to get desired output power in the stable operating region of the device. The other parameters like quality factor and beam pitch factor were chosen in accordance with the stability condition of the device using start oscillation current curves. Table 4.2 shows the finalized design parameters taken for analysis of 35 GHz, 200 kW four-cavity gyroklystron amplifier. This conceptual device design has been validated through the nonlinear analysis and 3D PIC simulation.

Figure 4.8 shows the phase bunching of electrons at different positions of interaction structure during the CRM interaction. The number of representative electrons in the beamlet is taken as 60, which are initially equally distributed around a Larmor orbit. From Fig. 4.8, it can be seen that these uniformly distributed electrons get bunched azimuthally as they move along the interaction region. At the inlet of input cavity all electrons are equally distributed all over the phase (0, $2\pi$) as shown in Fig. 4.8 (a). As the electrons drift through the input cavity, intermediate cavities and drift tubes, the electrons get azimuthally bunched

and a center of the bunch is formed as shown in Figs. 4.8 (b), 4.8 (c) and 4.8 (d). In the output cavity, these bunched electrons lose their energy to the RF and disperse in the phase space with reduced Larmor radii towards the outlet of the output cavity as shown in Figs. 4.8 (e) and 4.8 (f). The electronic efficiency of the device which is defined as the conversion of DC beam power to RF output power is calculated using equation 2.31. The axial field distribution and the electronic efficiency in the output cavity are shown in Fig. 4.9. It can be seen from Fig. 4.9 that when the output cavity of the designed gyroklystron operates at the fundamental harmonic, the resultant electronic efficiency is about 37.4%, and the corresponding output power is 215 kW.

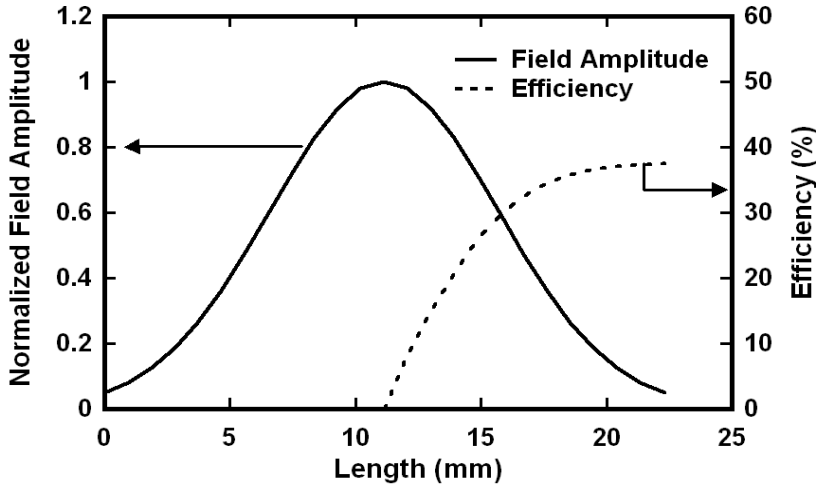


**Fig. 4.9** Normalized field distribution and electronic efficiency in the output cavity.

In Fig. 4.10, the output power variation has been observed with the electron transverse to axial velocity ratio ($\alpha$) for 0%, 5%, and 10% electron beam velocity spreads. The maximum output power is achieved at velocity ratio ($\alpha$) ~1.5 for 0% velocity spread as shown in Fig. 4.10. The RF output power decreases for higher as well as lower values of electron transverse to axial velocity ratio. Only the transverse velocity component of gyrating electron beam takes place in the beam-wave interaction and power transfer mechanism and thus the RF power reduces at the lower values of the $\alpha$. At higher values of $\alpha$ the RF output power decreases due to the operation of the device in the unstable region. It can also be seen from Fig. 4.10 with increasing velocity spread the output power

decreases. This happens because some of the electrons have lower energies and hence transfer lesser amount of energy to the RF.

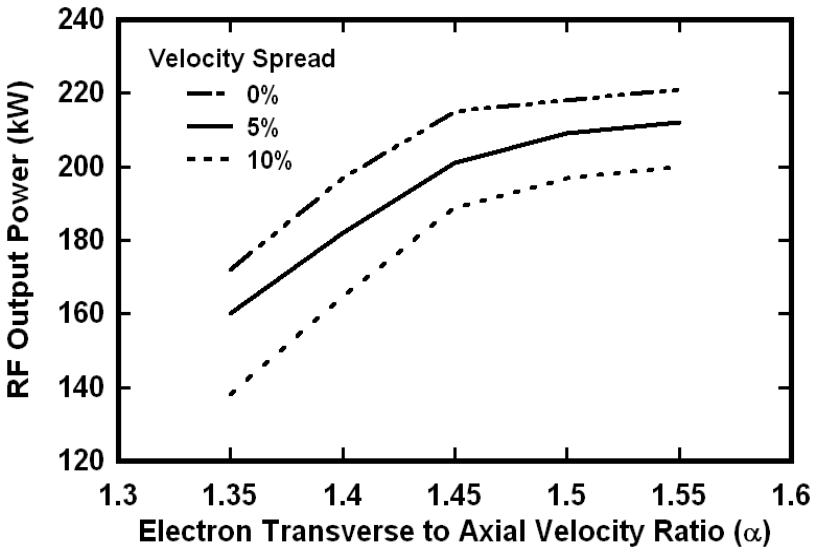


**Fig. 4.10** Output power variation with electron beam pitch factor (α) for different velocity spreads.

## 4.4 Device Simulation

In order to study the overall device performance and beam-wave interaction mechanism of a gyroklystron a commercially available 3D PIC simulation code 'MAGIC' has been used and method of its adaptation and reconfiguration is explained in this section. Typical, a four-cavity gyroklystron, designed using the methodology described in the previous section is taken here to describe the simulation process as well as to validate the device design. For device simulation, first the RF interaction structure of the device is modeled. Next, the RF cavity simulation is performed in the absence of electron beam to examine its electromagnetic behavior, like, operating mode, frequency, field profiles, etc. This is known as eigenmode or cold RF analysis. Then, the gyroklystron structure is simulated in the presence of electron beam (hot condition) to observe the RF output power, gain, efficiency, etc. The detailed procedure used in the 3D PIC simulation using commercial code 'MAGIC', for the beam absent (cold) RF cavity and beam present (hot) cavity analysis for studying the RF behavior in the gyroklystron amplifier is described below.

### 4.4.1 Modeling of the RF interaction structure

3-D RF structure of a four-cavity gyroklystron is first modeled and the cross-sectional view of model used for the simulation is shown in Fig. 4.11. The cylindrical coordinate system ($z$, $r$, $\theta$) is used here for modeling the structure. For meshing, the grid sizes during the simulation have taken as $\Delta z = \lambda/40$, $\Delta r = \lambda/40$, and $\Delta\theta = 15^0$. Due to symmetric nature of the RF interaction structure, the uniform meshing is made using the command existing in the code for the discretization of the structure to obtain fast converging results. As shown in Fig. 4.11, the present gyroklystron consists of four cylindrical cavities with input cavity length equal to 12.85 mm, input cavity radius equal to 5.6 mm, second and third cavities lengths are equal to 15.86 mm and radius equal to 5.5 mm. The output cavity has a length 23.14 mm and radius 5.3 mm. The cavities are isolated to each other with the help of drift tubes, which are at cutoff to the operating mode. The drift tube has a radius 4.1 mm and length 14.57 mm.

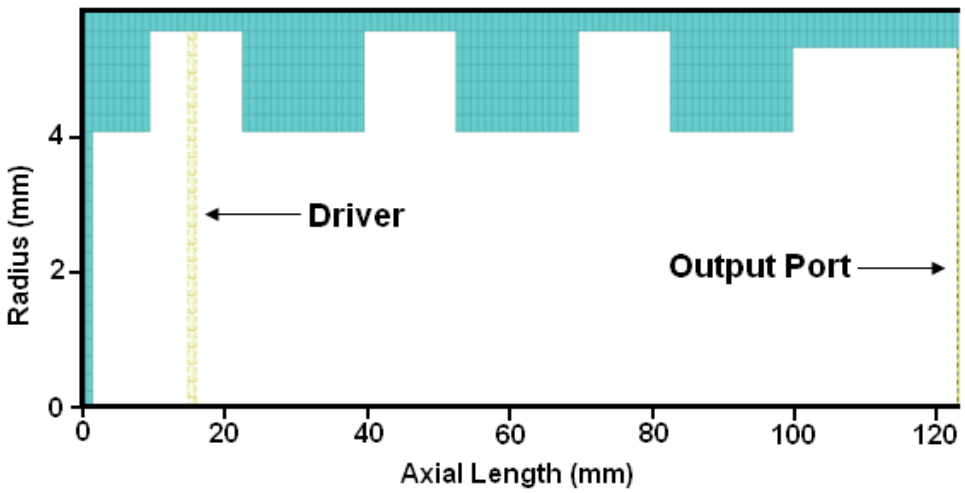


**Fig. 4.11** Cross-sectional view of the four-cavity gyroklystron RF interaction structure.

Material properties of the cavities wall are typically assigned metal (copper) to estimate the wall loading. RF cavities are externally loaded to achieve the desired quality factor. Drift tubes are externally loaded to avoid any cross-talk between the two cavities by absorbing the field leaked from cavities to drift region. A port at the end of the RF interaction structure has been assigned to observe the RF output power. The input cavity has been excited in the desired

mode corresponding to specific frequency and power with the help of a driver, i.e., a current-density source to drive electromagnetic fields in a local region of space.

### 4.4.2 RF cavity simulation (beam absent condition)

**— eigenmode study**

RF cavity simulation is carried out in the absence of electron beam with the help of the "eigenmode solver" of the simulation tool to study its electromagnetic behaviour. In eigenmode solver, an operator with predefined field configuration is applied to the resonant structure which give information about the excited eigenmodes, frequencies and electromagnetic fields configuration in a defined frequency range. Using this technique, the presence of desired mode inside the cavities is identified by observing the electric field pattern.

In Figs. 4.12-4.17 the results of eigenmode and eigenfrequency simulations are presented in various forms for 35 GHz resonant frequency. Figures 4.12 and 4.13 show the vector plot and the contour plot of the electric field intensity in the RF cavity. Figures 4.12 and 4.13 clearly show that there is one electric field peak along the radial direction of cavity and no peak along the azimuthal direction. This kind of electric field pattern confirms that the $TE_{01}$ mode is present inside the cavity.

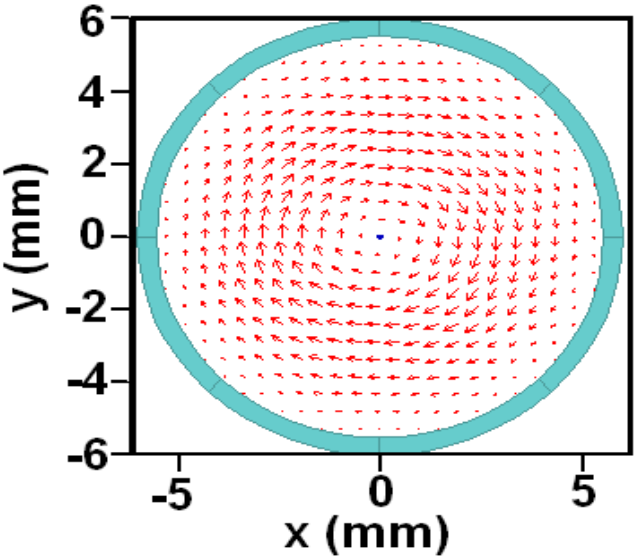


**Fig. 4.12** Vector plot of the electric field profile at the top cross-sectional view.

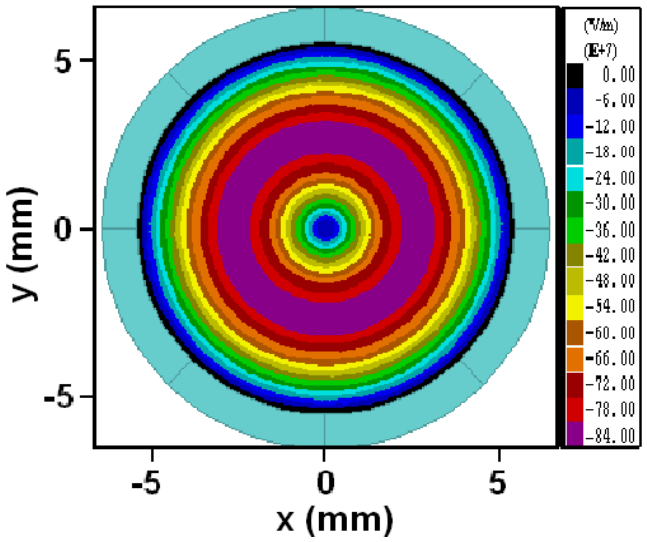


**Fig. 4.13** Contour plot of the electric field profile at the top cross-sectional view.

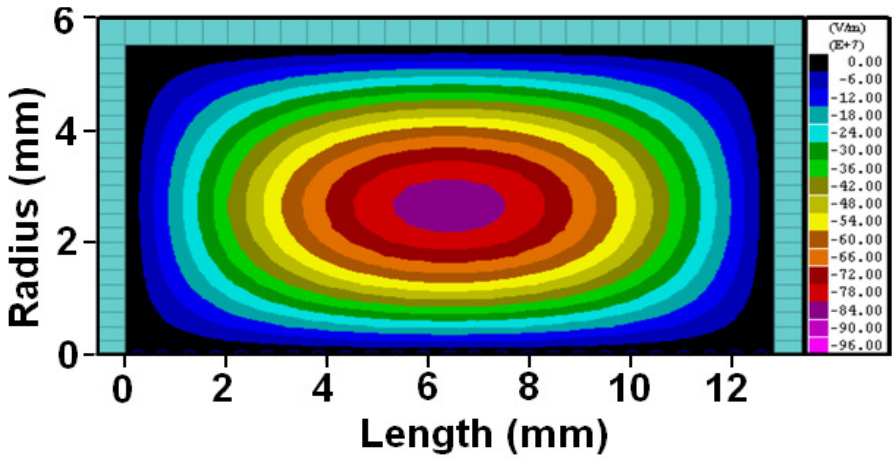


**Fig. 4.14** Contour plot of the electric field profile at the side cross-sectional view.

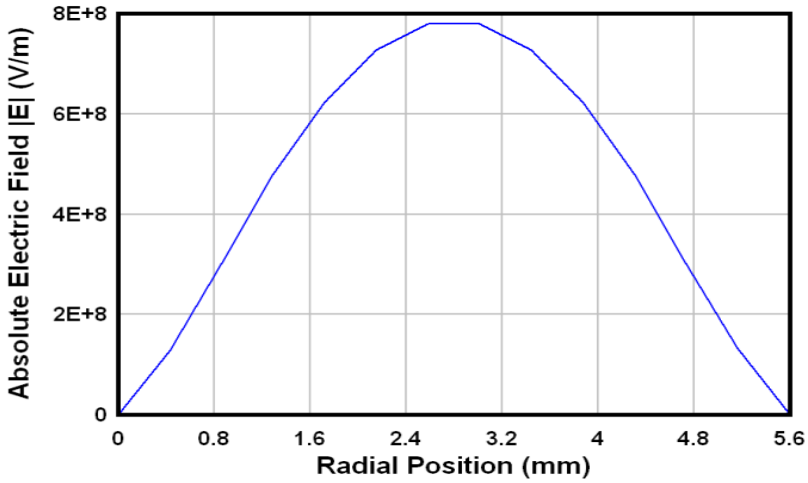


**Fig. 4.15** Radial variation of the electric field in the input cavity.

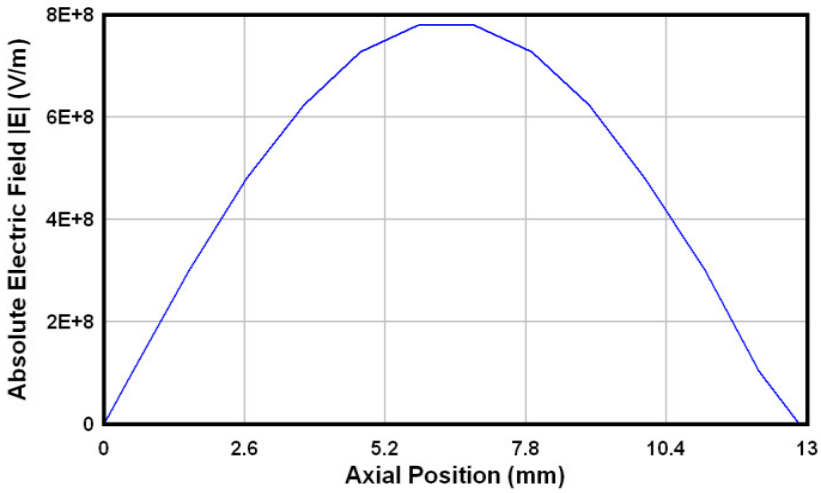


**Fig. 4.16** Axial variation of the electric field in the input cavity.

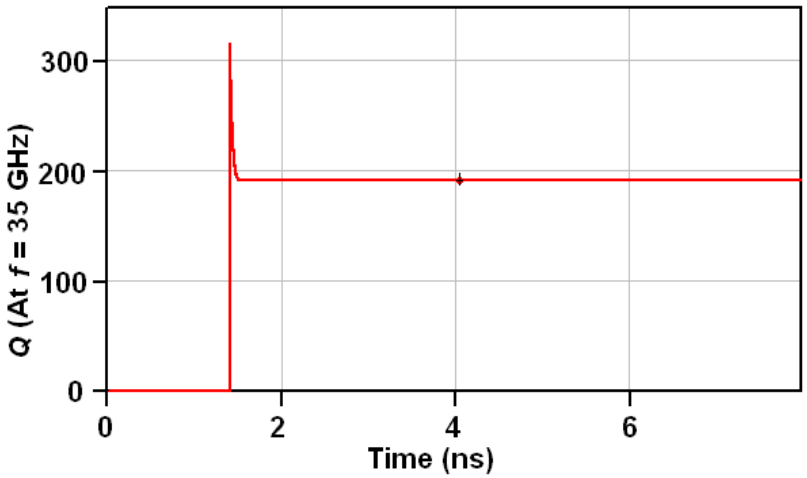


**Fig. 4.17** Loaded quality factor of the input cavity.

Figure 4.14 shows the side view of the contour plot of $TE_{01}$ mode. The radial and axial variations of the electric field magnitude are shown in Figs. 4.15 and 4.16, respectively. These figures identify the position of electric field maximum where the beam-wave interaction have to be taking place for optimum interaction. For estimation of the quality factor, cavity is loaded with the lossy ceramic and the cavity is excited by a current driver placed at its centre with 35 GHz frequency. The decay of EM energy inside the cavity is observed to estimate the loaded quality factor. From Fig. 4.17, the quality factor of the RF input cavity can be observed. For the present simulation, loaded quality factor is obtained as 192. It must be noticed that for the gyroklystron amplifier, loaded

quality factor is chosen at a lower level and is selected in such a way that device can operate into the stable region without possibility of moving into the oscillation region.

### 4.4.3 PIC simulation of the RF interaction structure (beam present condition) — beam-wave interaction study

The beam-wave interaction simulation is carried out for the estimation of operating frequency range, RF power output, gain, efficiency etc., in presence of the electron beam. For this purpose, a gyrating electron beam of the desired parameters is required. The gyrating electron beam of guiding center radius 2.65mm, with a electron beam pitch factor ($\alpha$) 1.45, beam current of 8.2A, and beam voltage of 70kV is introduced at the left end of the interaction structure using the emission command of the PIC code. Further, the external static magnetic field of 1.34T is applied axially along the interaction structure. Radiated output power is extracted at the output port of the output RF cavity. Figure 4.18(a) shows the cross-section of electron beamlets applied before interaction and Fig. 4.18(b) shows the cross-section of electron beamlets observed after interaction at the output port. Here, an electron beam of typically 24 electron beamlets have been selected to perform the simulation.

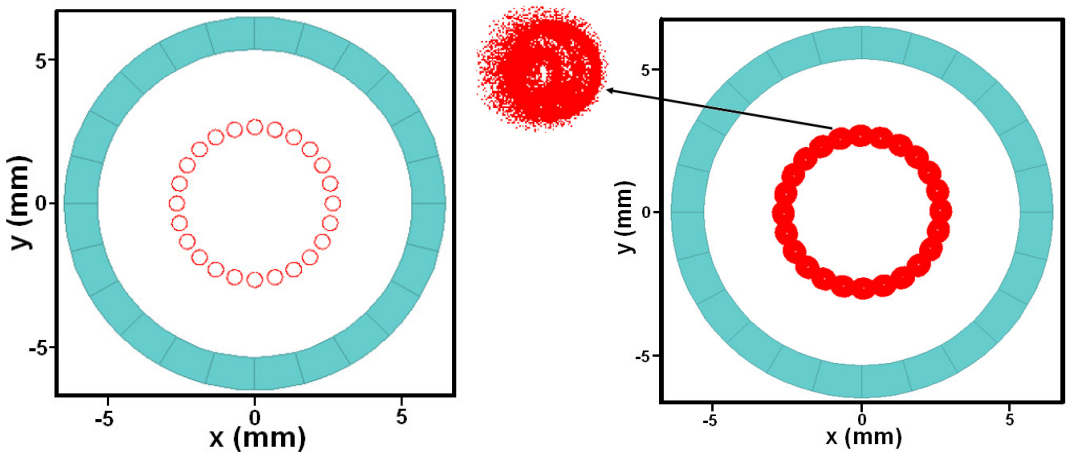


(a) (b)

**Fig. 4.18** Cross-section of electron beam (a) before interaction and (b) after interaction (inset shows a zoomed beamlet).

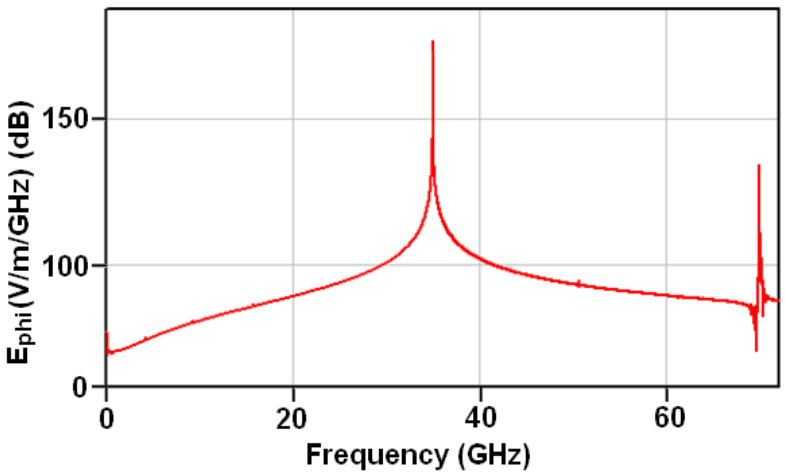


**Fig. 4.19** Observed frequency spectrum of electric field at the output cavity.

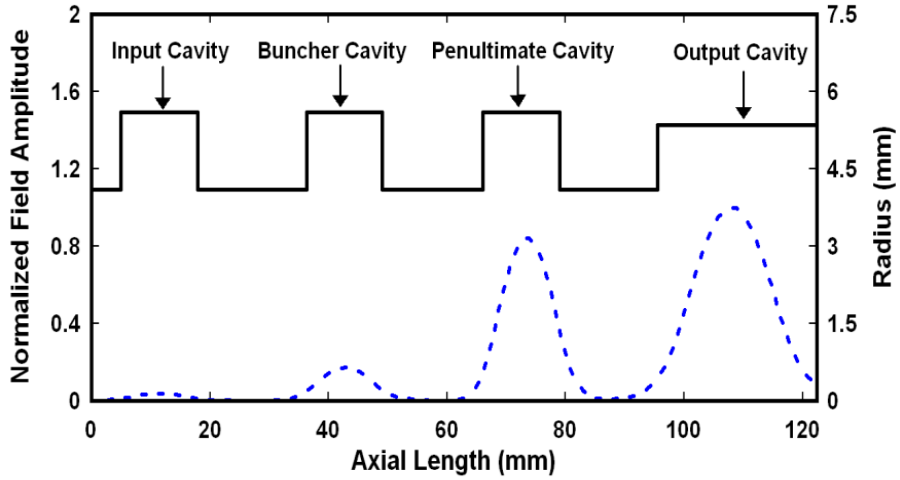


**Fig. 4.20** Variation of electric field along the axial length of the RF interaction structure.

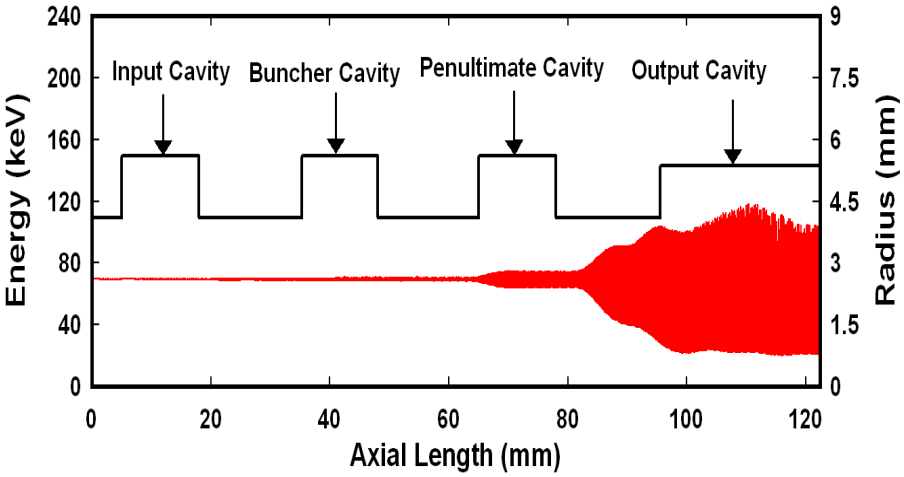


**Fig. 4.21** Evolution of particles energy along the RF interaction length.

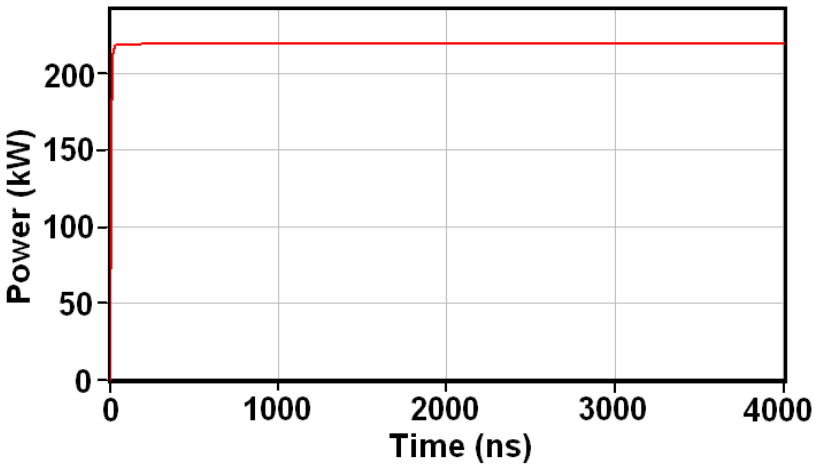


**Fig. 4.22** Temporal growth of RF output power at the output cavity.

The frequency of operation is validated by observing the Fourier transform of the azimuthal electric field of the time growing signal in output RF cavity (Fig. 4.19). The highest frequency peak is observed around 35GHz (fundamental mode) for $TE_{01}$ mode which confirms its operating frequency. The other noticeable peak of the electric field is found to be at 70GHz, corresponding to the second harmonic. It can be seen from Fig. 4.19, the amplitude peak of the second harmonic is nearly ~ 40dB lesser than the fundamental which ensure that in this operating region will be no mode competition. In Fig. 4.20, the electric field variation along the interaction length has been observed. It can be seen from the Fig. 4.20 that amplification of the signal is taking place as we move from input cavity to output cavity. The maximum field is observed at the centre of the output cavity whereas lesser field in other cavities. There is no field observed in the drift tubes which confirms the stable operation of the device.

Figure 4.21 shows the evolution of electrons energy along the axis. It can be seen that at the output end, the net electron energy is decreasing, indicating an energy transfer from the electron beam to the RF field. The RF input signal is applied to the input RF cavity to act as a driver (Fig. 4.11). In the simulation the RF input power is 6.5W. Figure 4.22 shows the time evolution of radiated output RF power corresponding to 6.5W RF input power, measured at the output port of the output RF cavity. The radiated power of 219kW reaches to saturation value at

30ns, corresponding to power conversion efficiency of 37% where beam voltage is 70kV and beam current is 8.2A.

## 4.5 Device Design and Simulation Validation

In order to estimate the gain and bandwidth of the device the curves for the RF output power variation with driver power and frequency have been obtained. Furthermore, to validate the device design and simulation results the comparison between the gain and bandwidth results obtained from nonlinear analysis and PIC simulation have been made.

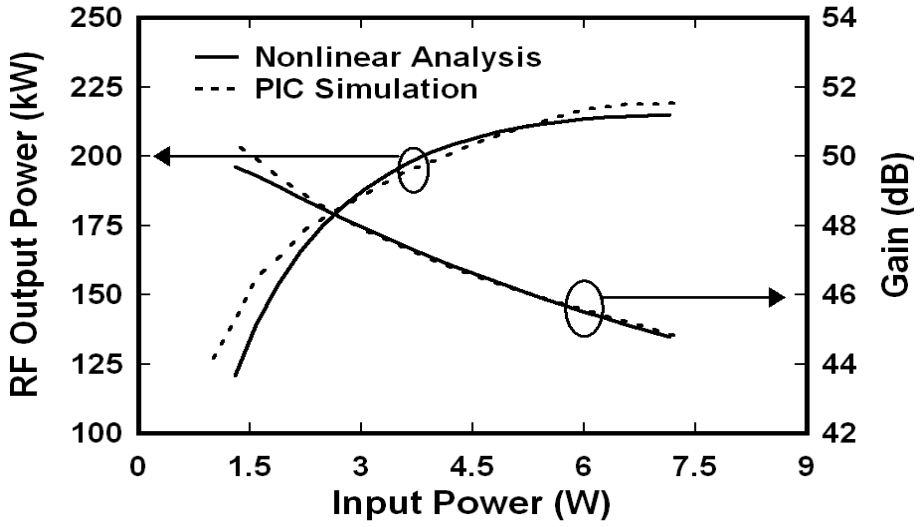


**Fig. 4.23** Dependence of RF output power and gain on driver power.

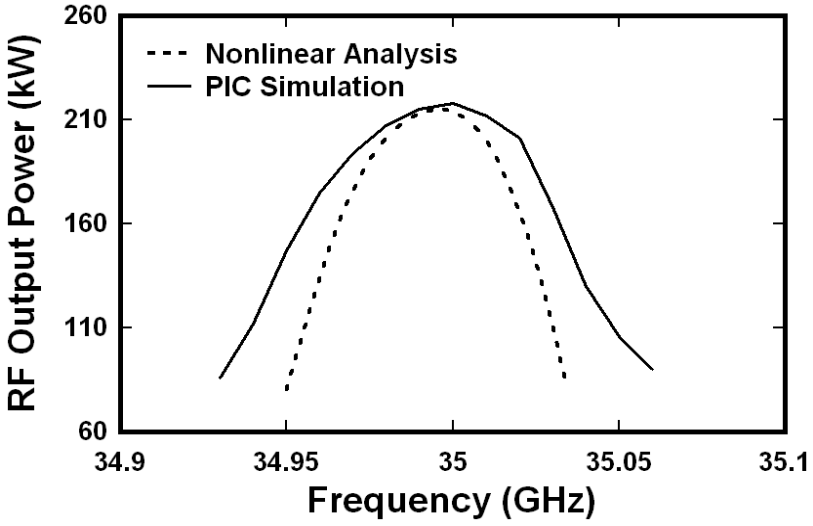


**Fig. 4.24** Dependence of RF output power on frequency.

The variation of output RF power and gain achieved as a function of input power using PIC simulation (Fig. 4.23) has been validated with the results obtained from the nonlinear analysis. The RF output power of the device through nonlinear analysis is calculated by making use of equations (2.30) and (2.31). First, the momentum and phase of all the electrons taken into consideration is calculated at the output end of the RF output cavity using equation (2.28). After this, the transverse efficiency is determined using equation (2.30) by taking the average of all the electrons momentum obtained at the output end over the initial phase angle of the electrons. Consequently, the computation of efficiency, output power, and gain has been made for the designed gyroklystron. As seen from the Fig. 4.23, the RF output power reaches at saturation at ~ 215kW for 6.5W drive power corresponding to 45.2dB gain in case of nonlinear analysis, and 219kW with 45.3dB gain obtained through the PIC simulation. The analytically obtained values of RF output power and gain are in agreement with the PIC simulation results within ±5%. The bandwidth calculation of the device is done by plotting the output power as a function of frequency (Fig. 4.24). Since, a gyroklystron amplifier utilizes a series of resonant cavities for its beam-wave interaction structure. Therefore, the bandwidth of the device is quite low. The 3dB bandwidth obtained through simulation for this device at center frequency 35GHz is ~0.1GHz (105MHz). The simulated values of bandwidth are found to be in agreement with the nonlinear analysis results within ~8%.

## 4.6 Parametric Analysis

It is very difficult to keep values of various parameters fixed, like magnetic field, beam voltage, cavity dimensions, quality factor, etc. used in nonlinear analysis and PIC simulation when we go for the actual fabrication and realization of the device. Considering this problem and to make the present analysis more practically useful, a rigorous parametric analysis (also called sensitivity analysis) is carried out in detail for the developed gyroklystron model.

Figures 4.25 - 4.28 show the output power and efficiency variation with respect to static magnetic field, beam current, beam voltage, and quality factor

respectively. The output power and efficiency increases approximately linearly with magnetic field up to 1.34T after this the output power and efficiency start decreasing. This is due to the shifting of the detuning parameter from its optimum value as detuning parameter is directly depends on the magnetic field (Fig. 4.25). As a result of which, the condition of synchronism between the transverse electronic motion and RF waves get deteriorates and a weak beam-wave interaction process takes place due to poor azimuthal bunching of the electrons.

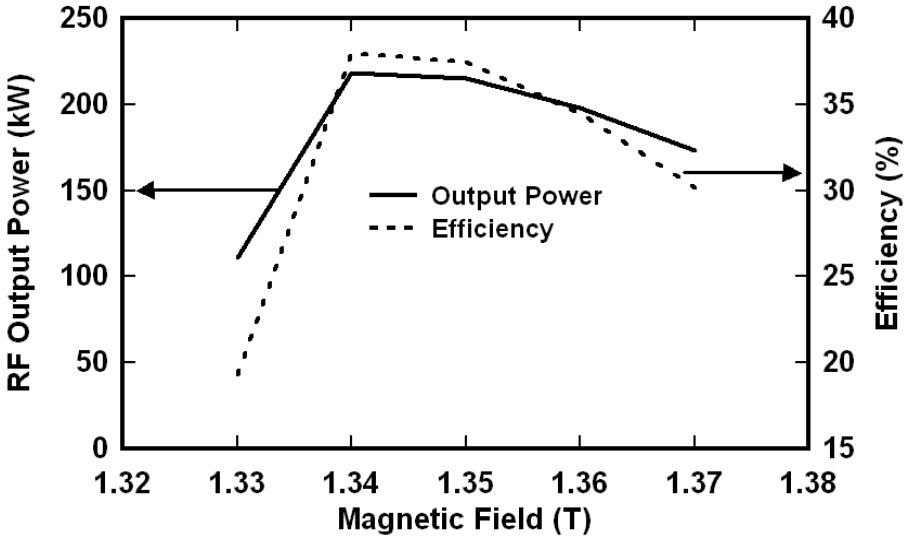


**Fig. 4.25** RF output power and efficiency variation with magnetic field.

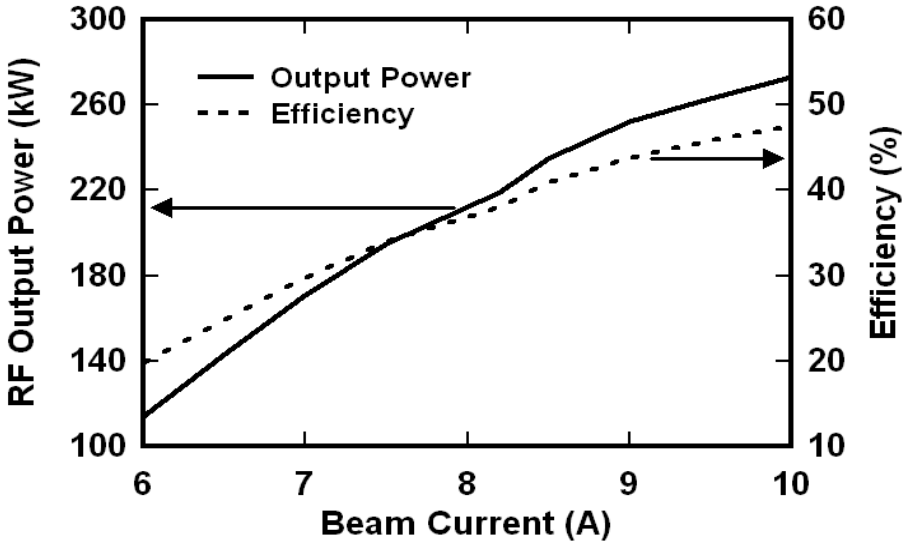


**Fig. 4.26** RF output power and efficiency variation with beam current.

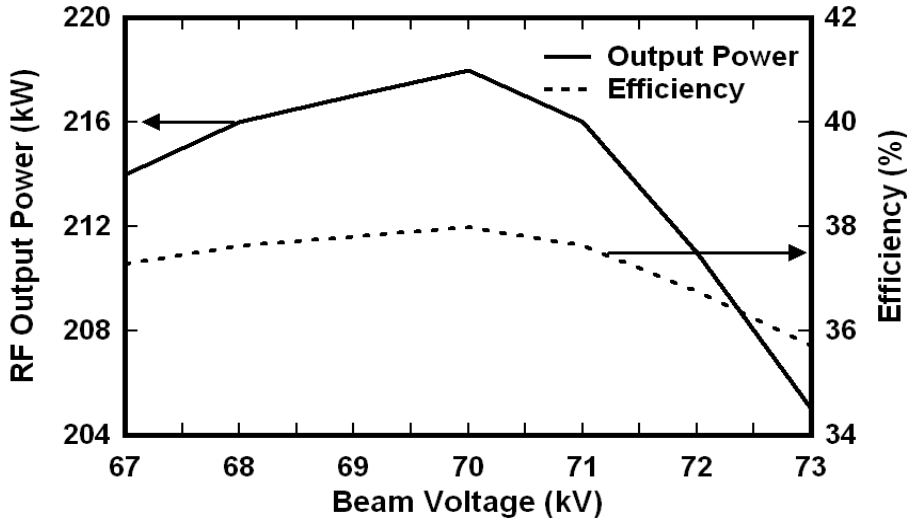


**Fig. 4.27** RF output power and efficiency variation with beam voltage.

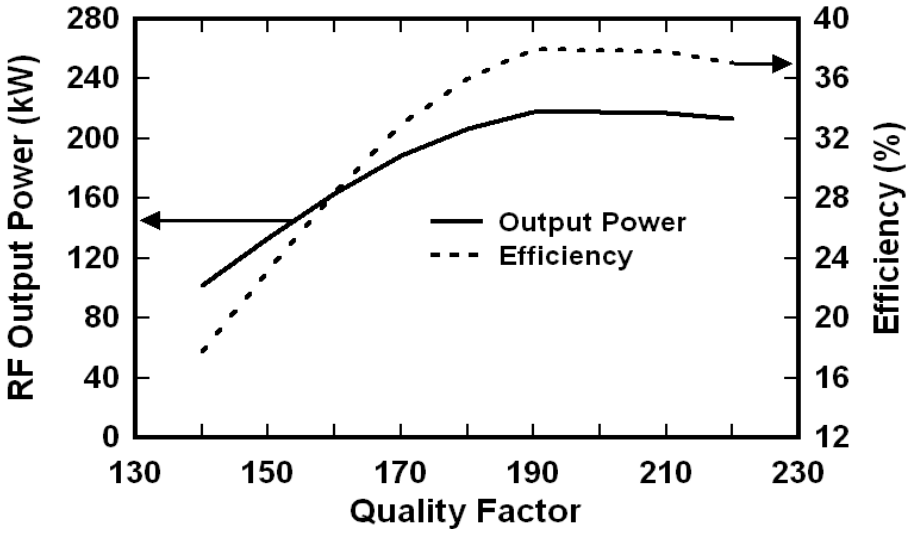


**Fig. 4.28** RF output power and efficiency variation with quality factor of output cavity.

In Fig. 4.26, it can be seen that the RF output power and efficiency increases as the beam current increases, which is due to the operation of the device near to start oscillation current. The effect of beam voltage and quality factor of the output cavity on output power and efficiency are shown in Figs. 4.27 and 4.28, respectively. The maximum RF output power is obtained around beam voltage 70kV and quality factor 190. The RF output power and efficiency of the device at higher values of $Q$ reduces due to decrease in the stability of the device because of the undesired oscillation caused by the operation of the device very close to start oscillation current.

## 4.7 Misalignment Study

During the assembling of the gyroklystron, the cavities and drift tubes may be displaced from the central (electron beam) axis. If the RF section (cavities and drift tubes) of gyroklystron amplifier is misaligned with respect to its original position, then the electron beam cannot be launched concentrically with respect to the electron beam axis. This misalignment affects the electron beam parameters such as, the beam launching position, velocity spread, which again affects the beam-wave interaction. Thus, the performance of a gyroklystron amplifier depends upon the alignment of RF cavities and drift tubes with respect to electron beam. Therefore, the sensitivity of gyroklystron amplifier on the misalignment of RF cavities and drift tubes in radial direction has been studied in detail.

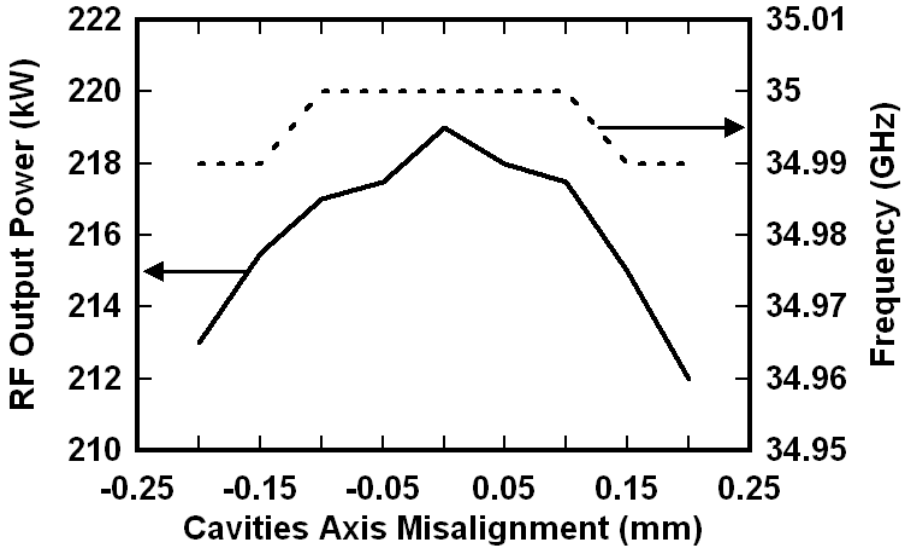


**Fig. 4.29** RF output power and frequency variations with cavities axis misalignment w.r.t. electron beam axis.

Figure 4.29 shows the RF output power and frequency variation with respect to cavities axis misalignment. The simulations are performed in the radial direction, and the results show a very small variation in the output power and frequency. Figure 4.30 shows the effect of cavities axis misalignment on the bandwidth of the device. The obtained results show that bandwidth of the device not affected much with the cavities axis misalignment.

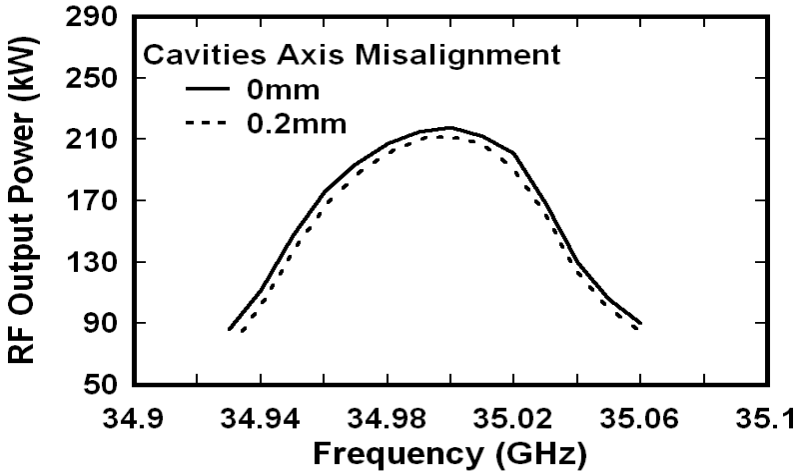


**Fig. 4.30** RF output power variation with driver frequency for different values of cavities axis misalignment.

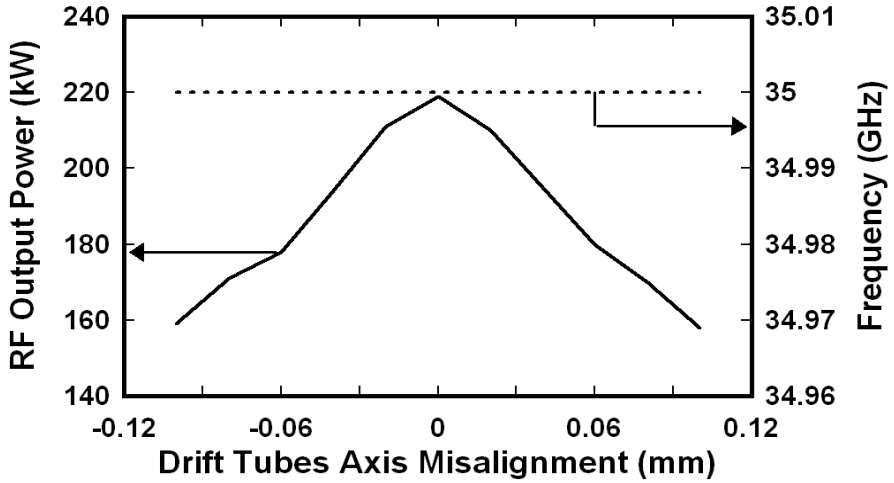


**Fig. 4.31** RF output power and frequency variations with drift tubes axis misalignment w.r.t. electron beam axis.

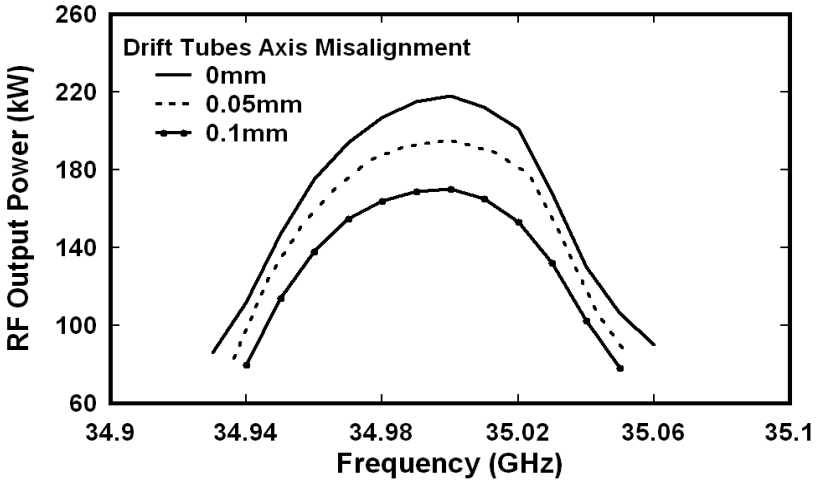


**Fig. 4.32** RF output power variation with driver frequency for different values of drift tubes axis misalignment.

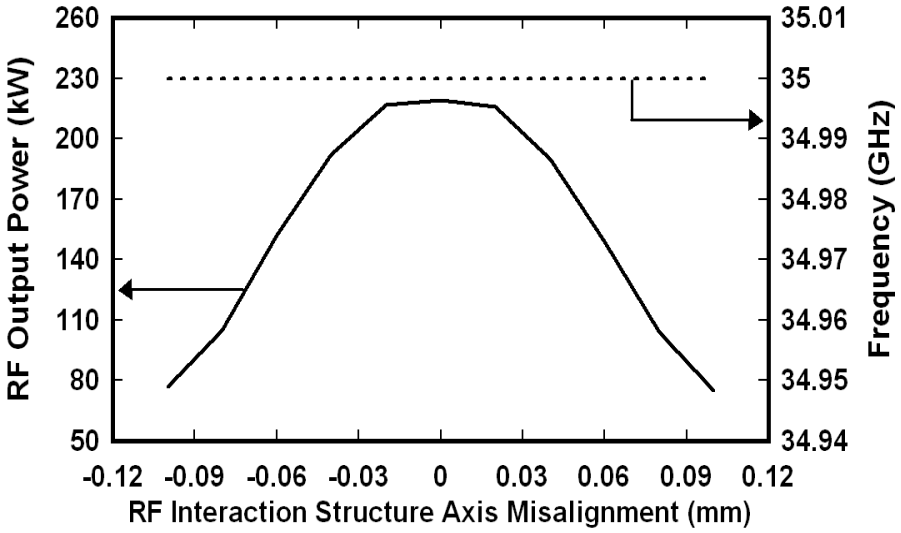


**Fig. 4.33** RF output power and frequency variations with RF interaction structure axis misalignment w.r.t. electron beam axis.

Figure 4.31 shows the results of drift tubes axis misalignment on the RF output power and frequency of the device. It can be seen from Fig. 4.31, that the frequency approximately remains constant whereas the RF output power decreases to a larger extent with drift tubes axis misalignment. In Fig. 4.32, the influence of drift tubes axis misalignment on bandwidth has been investigated. The bandwidth of the device has been not affected to a much extent with the drift tubes axis misalignment. The bandwidth of the device observed constant ~ 0.3% with the drift tubes axis misalignment increases from 0 to 0.1mm.

In Fig. 4.33, the effect of RF interaction structure axis misalignment on the device frequency and RF output power has been studied. It can be seen from Fig. 4.33 the RF output power of the gyroklystron amplifier is more sensitive to the RF section axis misalignment. Since, the output power of the device decreases from 218kW to 80kW with RF section misalignment to ±0.1mm. The frequency remains almost unaffected with the RF section misalignment.

## 4.8 Conclusion

In the present chapter, a comprehensive nonlinear analysis, device design methodology, and 3D PIC simulation of the gyroklystron have been presented. Taking resort of a typical Ka-band gyroklystron amplifier case, the conceptual device design has been described and validated by investigating the RF behavior

and values obtained through the nonlinear analysis as well as PIC simulation. A 3D device simulation has been performed both for the beam absent and beam present cases using a commercial PIC simulation code 'MAGIC'. The simulation procedure and beam-wave interaction investigation have been thoroughly described. Electric field patterns obtained through simulation confirms the device operation in the desired mode. Electron beamlets observed at the output port at the end of simulation shows the bunching mechanism of the particles. The energy distribution of all the electrons along the interaction length confirms the net energy transfer from beam to RF. The gyroklystron under investigation produces a stable output power of ~219kW at center frequency 35GHz with electronic efficiency 37% corresponding to ~45dB gain and 3dB bandwidth ~0.3%. Validation of results obtained here has been found in agreement of ~5% with the analytical results obtained through nonlinear analysis. In assembling of the various components of the gyroklystron some misalignment can occur. A practical case of the misalignment of the cavities axis, drift tube axis and both the axes is also investigated and found that the RF output power is more sensitive to the misalignment in comparison to the device bandwidth.